

Hepatic stellate cell-released CXCL1 aggravates HCC malignant behaviors through the MIR4435-2HG/miR-506-3p/TGFB1 axis

Shaling Li¹  | Xingwang Hu¹ | Songman Yu¹ | Panpan Yi¹ | Ruochan Chen¹ | Zebing Huang¹ | Yan Huang¹ | Yun Huang² | Rongrong Zhou¹ | Xuegong Fan¹

¹Hunan Key Laboratory of Viral Hepatitis, Department of Infectious Disease, Xiangya Hospital, Central South University, Changsha, China

²Department of Surgery, Xiangya Hospital, Central South University, Changsha, China

Correspondence

Rongrong Zhou and Xuegong Fan, Department of Infectious Disease, Xiangya Hospital, Central South University, 87# Xiangya Road, Changsha, Hunan, P.R. China.
Email: rr_xy1234@csu.edu.cn and xgfan@csu.edu.cn

Funding information

Ministry of Science and Technology international Cooperation Project, Grant/Award Number: 2015DFA31490; National Natural Science Foundation of China, Grant/Award Number: 81970523; Nature Science Foundation of Hunan Province, China, Grant/Award Number: 2020JJ4877, 2020JJ4932

Abstract

Hepatic stellate cell (HSC) activation is a critical event in the development of hepatic fibrosis and hepatocellular carcinoma (HCC). By the release of soluble cytokines, chemokines, and chemotaxis, HSCs affect HCC cell phenotypes through a complex tumor microenvironment. In this study, weighted gene co-expression network analysis (WGCNA) was used to identify the TGF- β signaling pathway as a key signaling pathway in Hep3B cells cultured in HSC conditioned medium. MIR4435-2HG is a hub lncRNA associated with the TGF- β signaling pathway and HSC activation. HSC-conditioned medium (CM) culture induced HCC cell malignant behaviors, which were partially reversed by MIR4435-2HG silencing. miR-506-3p directly bound to MIR4435-2HG and the 3'UTR of TGFB1. Similarly, overexpression of miR-506-3p also attenuated HSC-CM-induced malignant behavior of HCC cells. In HSC-CM cultured HCC cells, the effects of MIR4435-2HG knockdown on TGFB1 expression and HCC cell phenotypes were partially reversed by miR-506-3p inhibition. HSCs affected HCC cell phenotypes by releasing CXCL1. In an orthotopic xenotransplanted tumor model of HCC cells plus HSCs in mice, CXCR2 knockdown in HCC cells significantly inhibited tumorigenesis, which was partially reversed by MIR4435-2HG overexpression in HCC cells. In HCC tissue samples, the levels of CXCL1, TGF- β 1, and MIR4435-2HG were upregulated, while miR-506-3p expression was downregulated. In conclusion, HSC-released CXCL1 aggravated HCC cell malignant behaviors through the MIR4435-2HG/miR-506-3p/TGFB1 axis. In addition to CXCL1, the MIR4435-2HG/miR-506-3p/TGFB1 axis might also be the underlying target for HCC therapy.

KEYWORDS

CXCL1, hepatic stellate cells (HSCs), hepatocellular carcinoma (HCC), MIR4435-2HG, miR-506-3p, TGFB1

Abbreviations: cDNA, complementary DNA; CM, conditioned medium; CSC, cancer stem cell; EMT, epithelial to mesenchymal transition; FISH, fluorescence in situ hybridization; H&E, hematoxylin and eosin; HCC, hepatocellular carcinoma; HSCs, hepatic stellate cells; IF, immunofluorescent; IHC, immunohistochemical; LIHC, liver hepatocellular carcinoma; lncRNAs, long non-coding RNAs; miRNAs, microRNAs; RIP, RNA immunoprecipitation; TCGA, The Cancer Genome Atlas; WGCNA, weighted gene co-expression network analysis.

This is an open access article under the terms of the [Creative Commons Attribution-NonCommercial](https://creativecommons.org/licenses/by-nc/4.0/) License, which permits use, distribution and reproduction in any medium, provided the original work is properly cited and is not used for commercial purposes.

© 2022 The Authors. *Cancer Science* published by John Wiley & Sons Australia, Ltd on behalf of Japanese Cancer Association.

1 | INTRODUCTION

Hepatocellular carcinoma (HCC) accounts for 85% of primary liver malignancies and is one of the most prevalent primary malignant tumors, with a relatively high incidence, frequent recurrence and poor prognosis.¹ The close crosstalk between cancer cells and their surrounding microenvironment exerts a crucial effect on the regulation of tumor biological behavior.² Hepatic stellate cells (HSCs) are mysterious cells with multiple functions in the liver that secrete soluble cytokines, chemokines, and chemotaxis to form a complex tumor microenvironment.³ Through the tumor microenvironment, activated HSCs can induce the deregulation of several mutual signals between HSC and precancerous liver cells or liver cancer cells, and promote tumorigenesis, migration, invasion, and metastasis of tumors.^{4,5} For example, TGF β 1 and the TGF β /Smad signaling are important for the activation of HSC, leading to the epithelial to mesenchymal transition (EMT),⁶ maintaining the cancer stem cell (CSC)-like properties of epithelial tumor cells, and finally promoting HCC development and aggressiveness.^{7,8} Considering the crucial role of HSCs and their related tumor microenvironment in HCC pathogenesis, the study of its mechanism may provide novel strategies for HCC therapy.

Noncoding RNAs, including long non-coding RNAs (lncRNAs) and microRNAs (miRNAs), were originally regarded as “transcriptional noise”, which could form functional network modules together with noncoding RNAs and protein-coding RNAs, affecting the proliferation, apoptosis, migration, and invasion of cancer cells.^{9,10} Compared with traditional differentially expressed gene analysis, weighted gene co-expression network analysis (WGCNA) has successfully detected co-expressed modules and hub genes, miRNAs, and lncRNAs from various aspects.^{11,12}

In the present study, the TGF- β signaling was chosen based on integrative bioinformatics analyses and previous studies.^{13,14} WGCNA was performed and MIR4435-2HG (LINC00978) was identified as a hub lncRNA; the specific effects of MIR4435-2HG on HSC activation were investigated. Since miRNAs could mediate the crosstalk between lncRNA and mRNA,^{15,16} miR-506-3p was predicted to target MIR4435-2HG. The predicted targeting and the dynamic effects of the MIR4435-2HG/miR-506-3p axis were investigated. Finally, we examined the expression of key factors within tissues. Collectively, the experiments were designed to investigate the role and mechanism of the MIR4435-2HG/miR-506-3p axis in HCC cell behaviors caused by the HSC-mediated tumor microenvironment.

2 | MATERIALS AND METHODS

2.1 | Clinical sampling

With the approval of the Medical Ethics Committee of Xiangya Hospital, 12 paired HCC and adjacent noncancerous tissue specimens were collected from surgical tumor resection in the Xiangya

Hospital. Informed consent was obtained from all enrolled patients.

2.2 | Cell lineages

Hepatocellular carcinoma cell line Hep3B (CL-0102) and human hepatic stellate cell line LX-2 (CL-0560) were purchased from Procell. Huh7 cells were purchased from the Chinese Academy of Sciences Shanghai Cell Bank. SNU-449 cells were purchased from the ATCC. LX-2, SNU-449, and Huh7 cells were cultured in DMEM medium (Gibco) supplemented with 10% FBS (Invitrogen). Hep3B cells were cultured in MEM (Gibco) containing 10% FBS (Invitrogen). All cells were cultured at 37°C in 5% CO₂.

2.3 | Collection of conditioned medium

The HSC-CM was collected from confluent cells after 48 hours of culture in a complete medium. At this point, the HSC-CM was centrifuged and frozen at -20°C. A new aliquot was used for each experiment.

Recombinant CXCL1 (rCXCL1) protein was obtained from Abnova. rCXCL1 was added to the complete medium at a final concentration of 10 ng/ml and incubated for 48 hours.

2.4 | Cell transfection

Synthetic si-RNA pool of MIR4435-2HG and CXCL1, agomir-506-3p, antagomir-506-3p, si-CXCR2 1/2/3, and the corresponding negative controls (si-NC, agomir-NC, and antagomir-NC) were purchased from GenePharma. Target cells were transfected for 48 hours with siRNA, agomir, or antagomir using Lipofectamine 3000 (Invitrogen). The sequence is listed in Table S1.

2.5 | qRT-PCR

Total RNA was extracted and evaluated by qRT-PCR. For mRNA expression, the complementary DNA (cDNA) was synthesized using a RT-Master Mix (TaKaRa). The qRT-PCR after reverse transcription was then performed using a StepOnePlus RT PCR system (Applied Biosystems). As for the examination of miRNA levels, RNA was extracted using a miRNeasy isolation kit (Qiagen). The primers are listed in Table S1.

2.6 | Wound healing

Target cells were cultured in a six-well plates to a confluency of ~100%. After treatment with mitomycin C (1 mg/ml) for 1 hour, the cell layer was scratched with a 200- μ l sterile pipette. After washing,

the cells were incubated for 24 hours. Representative images were taken before and after 24 hours of incubation.

2.7 | Transwell for invasion

Target cells were cultured at a density of 10^5 cells/well in serum-free medium in the upper chamber containing Matrigel in Transwell. The bottom chamber was filled with 600 μ l of complete medium or HSC-CM. After 24 hours of incubation, the cells on the upper surface of the upper chamber (noninvasive) were removed, and the cells on the bottom surface (invasive) were fixed and stained with crystal violet and observed.

2.8 | Immunofluorescent staining

Target cells or tumor tissues were fixed with 4% paraformaldehyde, and then incubated with anti-E-cadherin (1:200, 20874-1-AP; Proteintech), anti-Vimentin (1:500, 10366-1-AP; Proteintech), anti-AFP (1:200, 14550-1-AP; Proteintech), or anti- α -SMA (1:500, 14395-1-AP; Proteintech) overnight at 4 °C, and then incubated with appropriate Alexa Fluor 488-labeled or Cy5-labeled secondary antibodies (Invitrogen) for 30 minutes at room temperature in the dark. The nuclei were counterstained with DAPI (Sigma-Aldrich). The cells were subsequently scanned with a fluorescent microscope.

2.9 | RNA fluorescence in situ hybridization

A specific DIG-labeled MIR4435-2HG probe (5'-DIG-CCAGATGCC GTTTTAGGGGACAGGATGTATTG-DIG-3) and DIG-labeled miR-506-3p probe (5'-DIG-TCTACTCAGAAGGGTGCCTTA-DIG-3) were obtained from Servicebio tech. After proteinase K digestion, the fixed cells were prehybridized with a hybridization solution and then incubated overnight with the MIR4435-2HG probe at 42 °C. After blocking, the cells were incubated with mouse anti-DIG-HRP for 50 minutes at 37 °C, and then with Cy3-TSA reagent for 5 minutes at room temperature in the dark. Later, the cells were incubated with the miR-506-3p probe, mouse anti-DIG-HRP, and FITC-TSA reagents as described above. Cell nuclei were stained with DAPI. MIR4435-2HG showed red inflorescence. miR-506-3p showed green inflorescence.

2.10 | Immunoblotting

Target cells were lysed using lysis buffer (Roche) containing protease inhibitors. Protein samples were collected and separated by SDS-PAGE (10%–12%) and transferred to polyvinylidene fluoride (PVDF) membranes (Beyotime). The membranes were first blocked with 5% bovine serum albumin (BSA), followed by primary antibodies against E-cadherin (20874-1-AP; Proteintech), Vimentin (10366-1-AP; Proteintech), TGF- β 1 (ab215715; Abcam), ZEB1 (66279-1-1G; Proteintech), Smad2 (12570-1-AP; Proteintech), p-Smad2 (#18338;

CST), Smad3 (66516-1-Ig; Proteintech), and p-Smad3 (1:2000, ab52903; Abcam) overnight at 4 °C. Then, membranes were incubated with secondary antibodies and visualized using enhanced chemiluminescent reagents (Beyotime). The relative protein expression was analyzed using ImageJ software.

2.11 | RNA immunoprecipitation assay

Hep3B cells (1×10^7) were lysed using an RNA immunoprecipitation (RIP) lysis buffer (Millipore). The cell lysates were then incubated with RIP immunoprecipitation buffer containing magnetic beads of human anti-argonaute2 (AGO2) antibody (Millipore) or negative control mouse IgG (Millipore). The samples were incubated with proteinase K. At the end of the incubation, the immunoprecipitated RNA was isolated and the levels of MIR4435-2HG and miR-506-3p were analyzed by qRT-PCR.

2.12 | Biotin-labeled RNA pulldown

HSC cells were seeded in a six-well plate and transfected with biotin-labeled miR-506-3p or scramble sequence using Lipofectamine 3000 for 48 hours. Cells were then harvested and lysed. Cell lysates were incubated with C-1 magnetic beads (Life Technologies) at 4 °C for 2 hours and then purified using an RNeasy Mini Kit (Qiagen). The level of MIR4435-2HG in the purified RNA was analyzed using qRT-PCR.

2.13 | Dual-luciferase reporter assay

The MIR4435-2HG fragment or TGFB1 3'UTR was cloned into Pscheck-2 (Promega) to construct wild-type MIR4435-2HG and TGFB1 3'UTR luciferase reporter vectors. Mutant-type MIR4435-2HG and TGFB1 3'UTR luciferase reporter vectors were generated by mutating the predicted miR-506-3p binding site within MIR4435-2HG or TGFB1 3'UTR after transfection into 293T cells. The luciferase activity was determined as previously described.¹⁷

2.14 | ELISA

The Human CXCL1 ELISA kit (DY275; R&D Systems) was used to determine the levels of CXCL1 in the culture medium according to the protocols.

2.15 | Hematoxylin and eosin, and immunohistochemical staining

Hematoxylin and eosin (H&E) and immunohistochemical (IHC) staining were used as described above for histological analysis.¹⁸ The clinical specimens were fixed with 4% paraformaldehyde in

PBS overnight, embedded in paraffin, and cut into 5- μ m-thick slices. The IHC analysis was performed with primary antibody against CXCL1 (1:500, ab89318; Abcam) and TGF- β 1 (1:500, ab215715; Abcam).

2.16 | Establishment of an orthotopic xenotransplanted tumor model of HCC in mice

Hep3B cells were transfected with lv-sh-NC, lv-shCXCR2 (Genechem) for 48 hours and then collected for orthotopic injection. BALB/c nude mice (SJA Laboratory Animal Co., Ltd) were divided into three groups: the Hep3B cells (transduced with lv-sh-NC)+HSC group ($n = 6$), the Hep3B cells (transduced with lv-sh-CXCR2)+HSC group ($n = 6$), and the Hep3B cells (transduced with lv-sh-CXCR2+MIR4435-2HG)+HSC group ($n = 6$). A total of 5×10^5 HSCs mixed with 1.5×10^6 Hep3B were suspended in 20 μ l PBS and injected orthotopically into the liver of mice. After 4 weeks, anesthetized mice were sacrificed and the tumor numbers were examined. Tumor tissues were collected and subjected to qRT-PCR and double-labeling immunofluorescence for AFP (HCC cell marker) and α -SMA (hepatic stellate cell activation marker) labeling.

2.17 | Statistics analysis

The results from at least three independent experiments were processed using GraphPad and expressed as mean standard deviation (SD). One-way analysis of variance (ANOVA) and Tukey's multiple comparison test or Student's *t*-test were used to assess the statistical significance of differences.

3 | RESULTS

3.1 | Deregulated signaling pathways in Hep3B cells cultured in HSC-conditioned medium based on GSE62455

The differentially expressed genes in HCC cells in response to normal culture medium (CM) and HSC-obtained conditioned medium (HSC-CM) were analyzed according to GSE62455 ($\log_2|FC| > 0.45$ and adjusted *p* value < 0.05). GSE62455, using Affymetrix GeneChip Human Gene 1.0 ST Array platform (HuGene10stv1_Hs_ENSG, Brainarray Version 12 CDF), contains gene expression profiles of paired samples of HSC and hepatocyte cell culture treated with CM of HSC cells to elucidate cell communication from HSC to HCC cells. We performed Kyoto Encyclopedia of Genes and Genomes (KEGG) signaling pathway enrichment annotation (Figure S1). Gene ontology (GO) function annotation (Figure S1) and Gene Set Enrichment Analysis (GSEA) (Figure S1) were used to analyze differentially expressed genes in Hep3B cells treated with CM or HSC-CM, with data from GSE62455. Figure S1 shows that differentially expressed genes

were enriched in TGF- β , cellular response to TGF- β , or TGF- β downstream EMT signaling.

3.2 | WGCNA identifying hub genes associated with HSC effects on HCC cells

Next, we performed WGCNA analysis on differentially expressed genes reported in GSE62455, which contained 15 HSC samples. Fifteen HCC cell samples were treated with HSC-CM, and four HCC cell samples were treated with CM to identify the hub genes associated with HSC-CM-caused changes in HCC cells. First, hierarchical clustering was performed on all samples and outliers (15 HSC samples) were pruned (Figure S2A). Next, we selected the appropriate adjacency matrix weight parameter to ensure scale-free distribution as much as possible. The parameter β is the square of the coefficient R and ranges from 1 to 20. A linear model of the logarithm of the connectivity of a node $\log(i)$ and the logarithm of the probability of the occurrence of a node $\log(p(i))$ was established. The detected network parameters are shown in Figure S2B. When $\beta = 6$, the evaluation parameter of the scale-free network was close to 0.9, and the mean connectivity was close to 0 (Figure S2B). Thus, $\beta = 6$ has a good discriminant degree and was used for further analysis. The best β value was calculated by the powerEstimate (pickSoft Threshold function).

As shown in the cluster dendrogram in Figure S2C, the 4485 differentially expressed genes formed 11 gene co-expression modules. They are represented in black (230) turquoise (783), brown (657), green (523), greenish-yellow,⁴⁰ magenta (186), pink (220), purple (53), red (274), blue (888) and yellow (565) colors. Gray represented that genes were not successfully clustered. Next, the hierarchical clustering method was used to calculate the network topological overlap topological overlap matrix (TOM) (Figure S2D). A darker color indicates a higher correlation or topological overlap between genes, which indicates a closer relationship between genes. On the upper left of the figure are the gene co-expression modules shown in the cluster dendrogram. From the network heatmap, the blue module was the most associated with the changes caused by HSC-CM (Figure S2D).

The 888 genes clustered in the blue module were further analyzed. Among them, there were 12 lncRNAs, ANXA2P1, DLGAP1-AS1, LINC01124, MIR4435-2HG, MSL3P1, NMRAL2P, PSMB8-AS1, RNU5E-1, SNORD116-24, SNORD116-6, SNORD116-8 and ZFAS1, respectively. Of these, five lncRNAs, MIR4435-2HG (upregulated), LINC01124 (downregulated), DLGAP1-AS1 (upregulated), PSMB8-AS1 (upregulated), and NMRAL2P (downregulated), were significantly changed by HSC-CM. MIR4435-2HG was the most upregulated lncRNA (Table S2).

GSE62455 confirmed that both MIR4435-2HG and TGFB1 expression were shown to be dramatically increased within HSC-CM-stimulated HCC cells than control CM-treated HCC cells (Figure S2E,F). Moreover, MIR4435-2HG was positively correlated with TGFB1 expression in samples (Figure S2G). MIR4435-2HG has been identified as a hub lncRNA associated with HSC-CM-caused changes in HCC cells.

3.3 | Effects of HSC-CM on HCC cells

The specific effects of HSC-CM on HCC phenotypes were examined. In Hep3B cells, consistent with online dataset results, FISH assay and qRT-PCR results showed that HSC-CM treatment significantly upregulated MIR4435-2HG levels (Figure 1A,B). The TGFB1 expression was also increased (Figure 1C). As for the cellular functions, HSC-CM treatment significantly promoted HCC malignant features through enhancing cell migration (Figure 1D) and cell invasion (Figure 1E). Consistent with the enhanced invasiveness of HCC cells, the protein content of E-cadherin was decreased, whereas vimentin was increased by HSC-CM treatment (Figure 1F). These data confirmed that HSC-CM treatment induced upregulation of MIR4435-2HG and TGFB1. In the meantime, HSC-CM enhanced HCC cell malignant behaviors.

Moreover, concerning HCC cells, the specific effects of HSC-CM on another two HCC cell lines, huh-7 and SNU-449, were investigated. As shown in Figure S3, HSC-CM enhances the malignant behaviors of huh-7 and SNU-449 cells, including cell migration (Figure S3A) and cell invasion (Figure S3B). Regarding the metastatic markers, the protein content of E-cadherin was decreased, whereas vimentin was increased by HSC-CM treatment in huh-7 and SNU-449 cells (Figure S3C). The changes in cellular phenotypes were similar to those of Hep3B cells, suggesting that the role of HSC-CM in HCC could be regarded as universal.

3.4 | MIR4435-2HG silencing inhibits HSC-CM-induced HCC cell malignant behaviors

Since HSC-CM induces MIR4435-2HG upregulation in HCC cells, we achieved MIR4435-2HG silencing in Hep3B cells and investigated the specific effects of MIR4435-2HG silencing on the phenotypes of HCC cells. The si-MIR4435-2HG was transfected to induce MIR4435-2HG silencing and qRT-PCR was performed to verify MIR4435-2HG expression (Figure 2A). Then, we transfected Hep3B cells with si-NC/si-MIR4435-2HG and cultured them with CM or HSC-CM to detect changes in the cell phenotypes and changes in key biomarkers. As for cellular functions, MIR4435-2HG silencing significantly inhibited the capacity of cells to migrate (Figure 2C) and to invade (Figure 2D) under either HSC-CM or control CM. HSC-CM-induced HCC cell migration and invasion were partially attenuated by MIR4435-2HG silencing (Figure 2C,D). HSC-CM decreased E-cadherin and increased vimentin, whereas MIR4435-2HG silencing exerted the opposite effect on EMT biomarkers. MIR4435-2HG silencing partially attenuated HSC-CM-induced changes in E-cadherin and vimentin (Figure 2B). As for TGF- β 1 and TGF- β /Smad signaling, HSC-CM increased TGF- β 1 and ZEB1 protein contents and promoted Smad2 and Smad3 phosphorylation (Figure 2E), both of which were all partially attenuated by MIR4435-2HG silencing (Figure 2E).

3.5 | miR-506-3p directly targets MIR4435-2HG and TGFB1 3'UTR

MIR4435-2HG silencing partially reversed the inducible effects of HSC-CM on TGF- β /Smad signaling activation, suggesting that TGFB1 might be downstream of MIR4435-2HG. Considering that miRNAs mediated the crosstalk between lncRNA and mRNA,^{15,16} we next used TargetScan, StarBase V3, miRDB, and DIANA tools to predict miRNAs that might target the 3'UTR of TGFB1 and the prediction results intersected in miR-506-3p (Figure 3A). Importantly, lncTar demonstrates that miR-506-3p can target MIR4435-2HG. Thus, we first examined the subcellular localization of miR-506-3p and miR-506-3p expression levels within HCCs in response to CM or HSC-CM. Figure 3B shows that miR-506-3p was localized at the cytoplasm, and the fluorescent signal intensity representing miR-506-3p was decreased by HSC-CM incubation. Furthermore, qRT-PCR also indicated that HSC-CM treatment significantly downregulated miR-506-3p expression (Figure 3C). Next, agomir-506-3p/antagomir-506-3p transfection achieved miR-506-3p overexpression/inhibition in Hep3B cells, and the expression level of miR-506-3p was determined by qRT-PCR (Figure 3D). In Hep3B cells, the overexpression of miR-506-3p downregulated and the inhibition of miR-506-3p upregulated MIR4435-2HG expression (Figure 3E). Similarly, in Hep3B cells, MIR4435-2HG knockdown induced by si-MIR4435-2HG significantly upregulated miR-506-3p expression (Figure 3F). In the meantime, miR-506-3p overexpression decreased, whereas miR-506-3p inhibition increased TGF- β 1 protein contents (Figure 3G).

Next, we constructed wild-type and mutant-type TGFB1 3'UTR and MIR4435-2HG luciferase reporter vectors, and co-transfected them to 293T cells with agomir-506-3p or antagomir-506-3p, respectively. We determined the luciferase activity. Figures 3H,I shows that, when co-transfected with wt-TGFB1 3'UTR or wt-MIR4435-2HG, the overexpression of miR-506-3p suppressed, whereas the inhibition of miR-506-3p enhanced the luciferase activity; when co-transfected with mut-TGFB1 3'UTR or mut-MIR4435-2HG, both miR-506-3p overexpression and inhibition failed to change the luciferase activity. Furthermore, RIP assay was performed using anti-IgG or anti-AGO2. Figure 3J shows that miR-506-3p and MIR4435-2HG levels in immunoprecipitate by anti-AGO2 were significantly higher than that in anti-IgG immunoprecipitate. Biotin-labeled RNA pulldown was performed using the biotin-labeled miR-506-3p. Figure 3K shows that the relative enrichment of MIR4435-2HG was remarkably higher in the biotin-labeled miR-506-3p group compared with the biotin-labeled scrambled control. Moreover, the FISH assays further confirmed that both MIR4435-2HG and miR-506-3p were mainly localized at the cytoplasm, and the fluorescent signal representing MIR4435-2HG and miR-506-3p existed in the same region (Figure 3L). In summary, miR-506-3p might target TGFB1 and MIR4435-2HG, respectively.

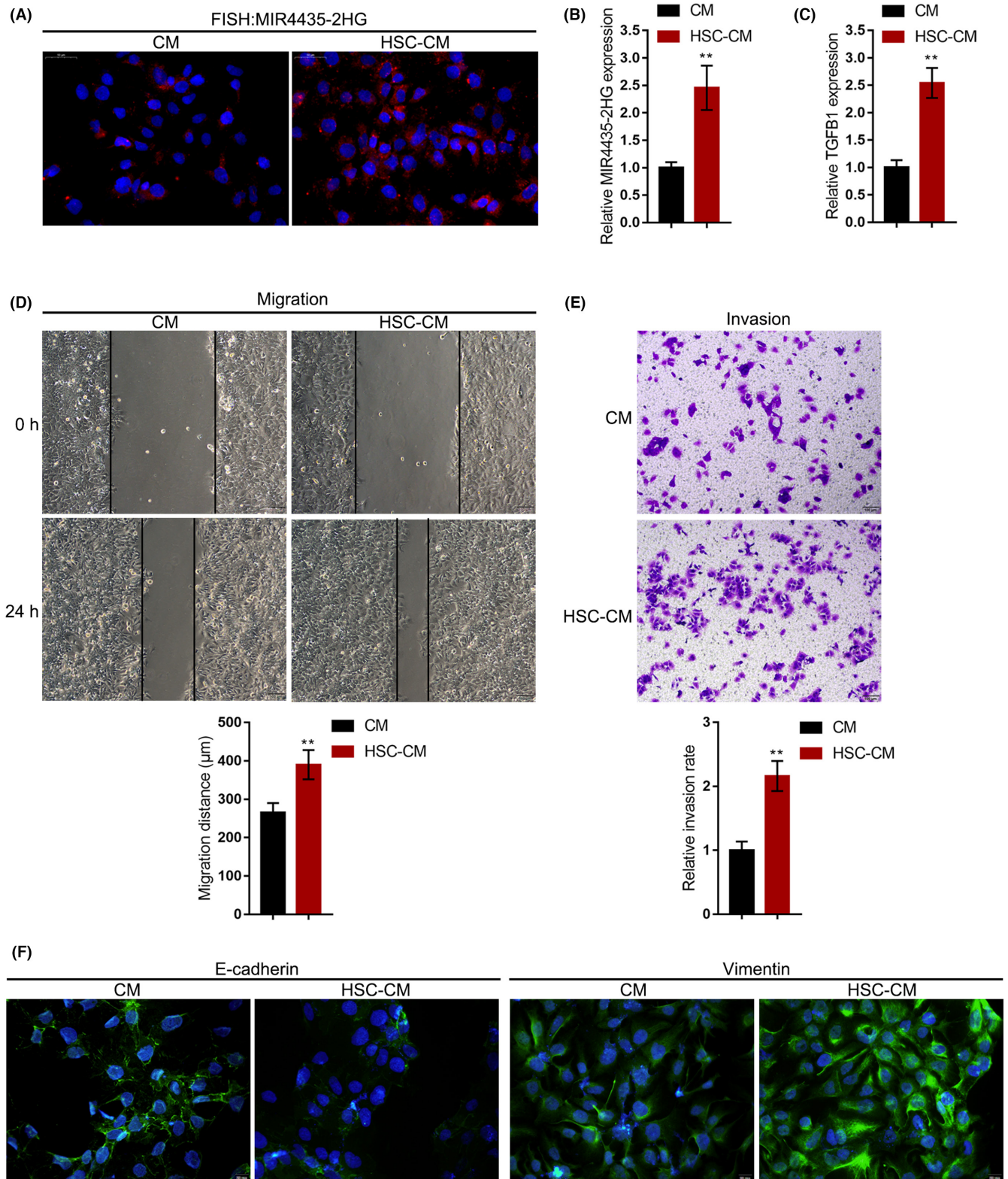


FIGURE 1 Effects of HSC-CM on HCC cells. Hep3B cells were cultured with a control medium (CM) or HSC-CM and examined for the expression levels of MIR4435-2HG and TGFB1 by FISH assays or qRT-PCR (A–C). Cell migration by wound healing assay (D). Cell invasion by Transwell assay (E). Protein content and distribution of E-cadherin and vimentin by immunofluorescent staining (F). ** $p < 0.01$.

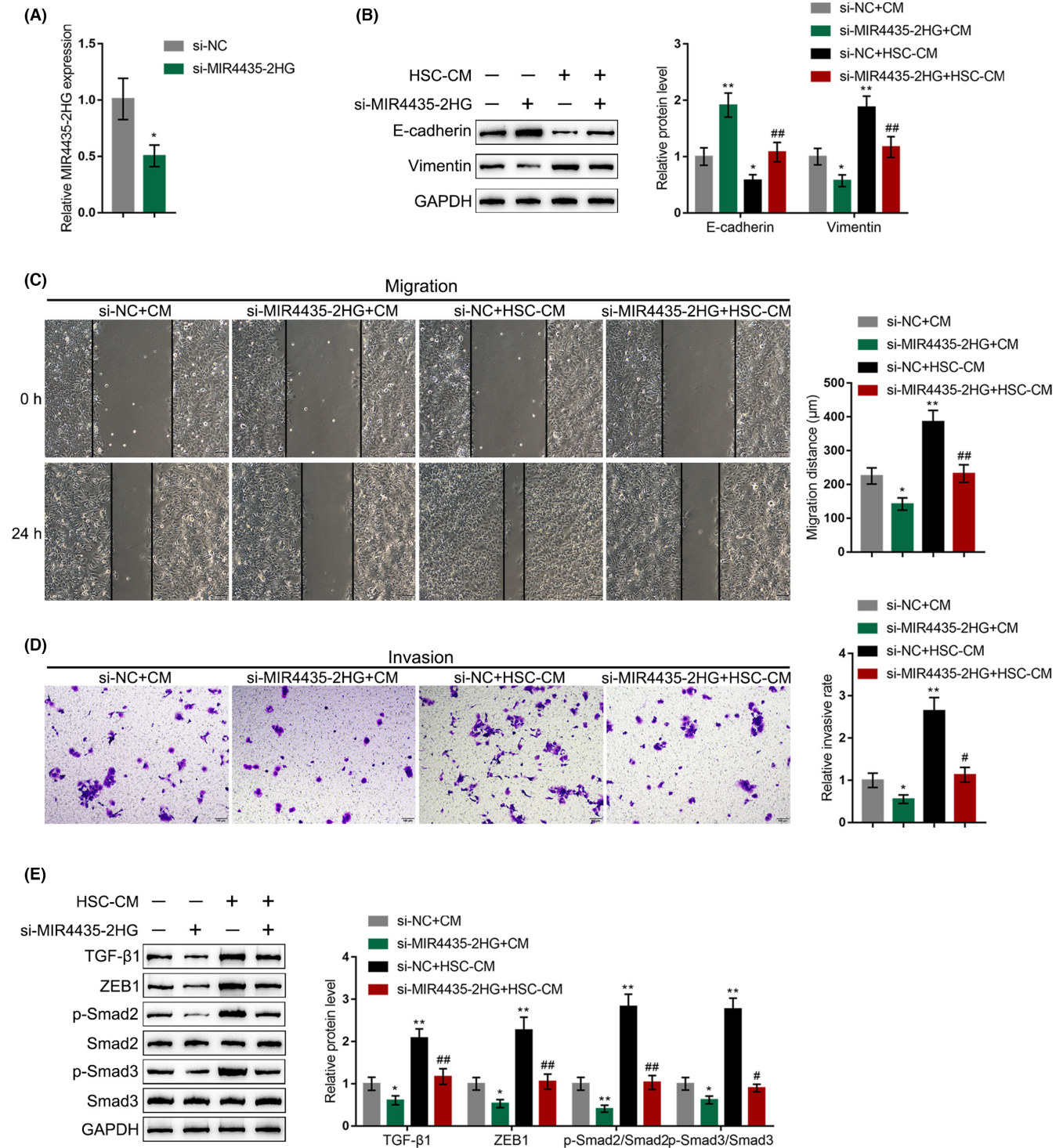


FIGURE 2 MIR4435-2HG silencing inhibits HSC-CM-induced HCC cell malignant behaviors. (A) MIR4435-2HG silencing was achieved in Hep3B cells by transfecting si-MIR4435-2HG. The expression of MIR4435-2HG was verified by qRT-PCR. Hep3B cells were transfected with si-NC or si-MIR4435-2HG, cultured with CM or HSC-CM, and examined for protein levels of E-cadherin and vimentin by immunoblotting (B), cell migration by wound healing assay (C), cell invasion by Transwell assay (D), and protein levels of TGF-β1, ZEB1, p-Smad2, Smad2, p-Smad3, and Smad3 by immunoblotting (E). * $p < 0.05$, ** $p < 0.01$, compared with the si-NC+CM group; # $p < 0.05$, ### $p < 0.01$, compared with the si-NC+HSC-CM group.

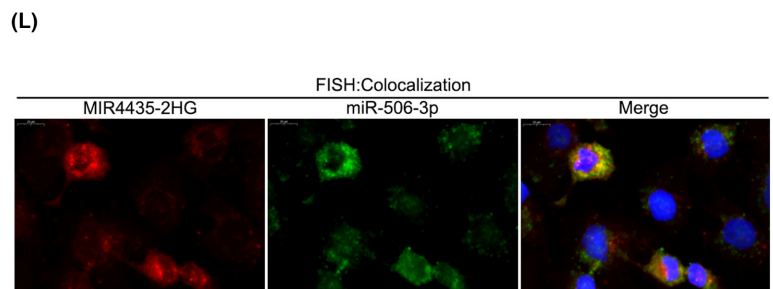
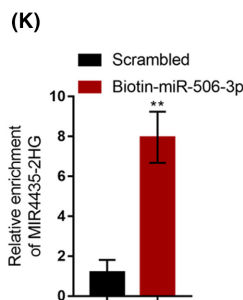
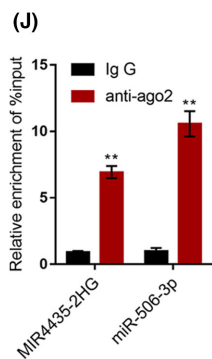
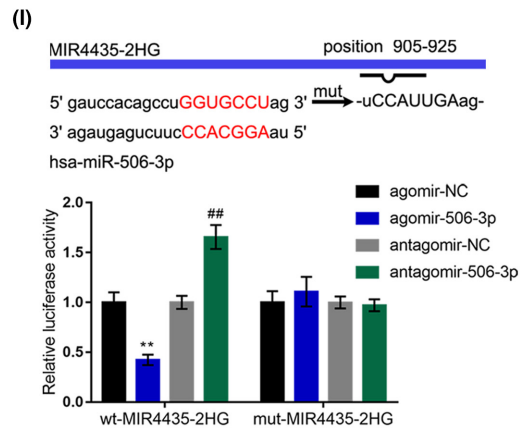
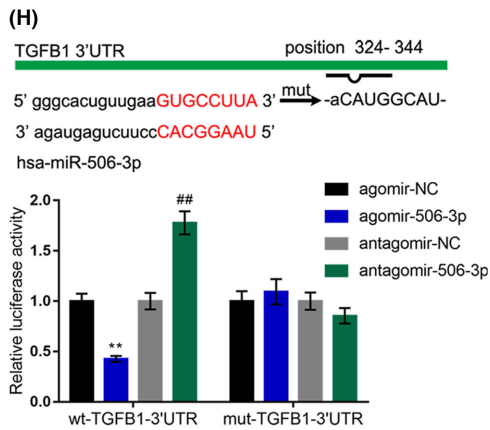
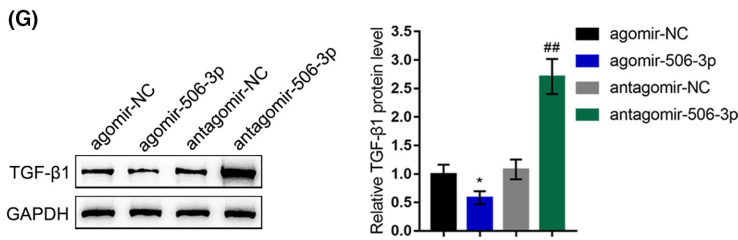
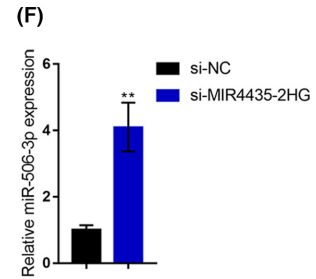
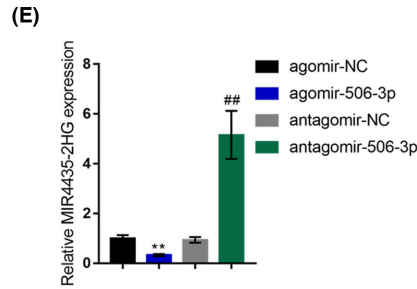
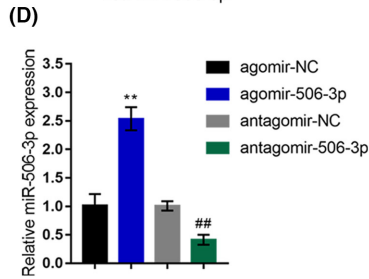
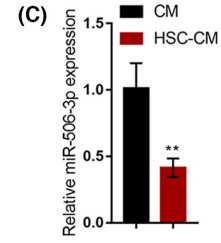
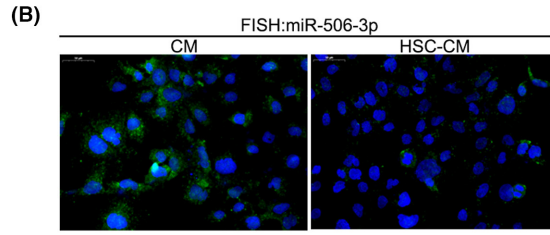
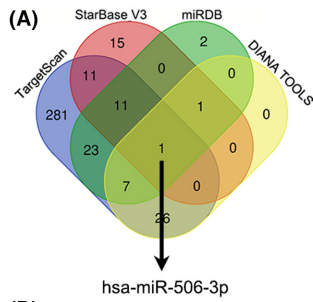


FIGURE 3 miR-506-3p directly binds to MIR4435-2HG and the 3'UTR of TGFB1. (A) TargetScan, StarBase V3, miRDB, and DIANA tools were used to predict miRNAs that might target the 3'UTR of TGFB1 and the prediction results intersected in miR-506-3p. (B) The subcellular localization of miR-506-3p and (C) miR-506-3p expression levels within HCCs in response to CM or HSC-CM were examined using FISH and qRT-PCR. (D) miR-506-3p overexpression or inhibition was achieved in Hep3B cells by transfecting agomir-506-3p or antagomir-506-3p. miR-506-3p expression was examined by qRT-PCR. (E) Hep3B cells were transfected with agomir-506-3p or antagomir-506-3p and examined for the expression levels of MIR4435-2HG by qRT-PCR. (F) Hep3B cells were transfected with si-MIR4435-2HG and examined for the expression levels of miR-506-3p by qRT-PCR. (G) Hep3B cells were transfected with agomir-506-3p or antagomir-506-3p and examined for the protein levels of TGF- β 1 by immunoblotting. (H, I) Wild-type and mutant-type TGFB1 3'UTR and MIR4435-2HG luciferase reporter vectors were constructed and co-transfected to 293T cells with agomir-506-3p or antagomir-506-3p. The luciferase activity was examined. (J) RIP assay was performed using anti-IgG or anti-AGO2. The levels of miR-506-3p and MIR4435-2HG in immunoprecipitate were examined. (K) Biotin-labeled RNA pull-down was performed using biotin-labeled miR-506-3p, and the level of MIR4435-2HG in the pulled-down complex was determined by qRT-PCR. (L) The colocalization of MIR4435-2HG and miR-506-3p was determined by FISH assays. * $p < 0.05$, ** $p < 0.01$, ### $p < 0.01$.

3.6 | miR-506-3p overexpression attenuates the effects of HSC-CM on HCC cells

After confirming the binding of miR-506-3p to TGFB1 and MIR4435-2HG, respectively, the present study investigated the function of miR-506-3p within HSC-CM effects on HCC cells. Similar to MIR4435-2HG silencing, miR-506-3p overexpression also inhibited the migration and invasion capacity of HCC cells and attenuated the promotive effects of HSC-CM on the aggressiveness of HCC cells (Figure 4A,B). Consistently, the overexpression of miR-506-3p downregulated the contents of vimentin, TGF- β 1 and ZEB1, inhibited Smad2 and Smad3 phosphorylation and upregulated E-cadherin expression, as well as attenuating the effects of HSC-CM on these proteins (Figure 4C,D). These data suggest that miR-506-3p overexpression significantly attenuates HSC-CM-enhanced HCC cell aggressiveness and TGF- β /Smad signaling activation, similar to MIR4435-2HG silencing.

3.7 | Dynamic effects of MIR4435-2H and miR-506-3p on TGF- β 1 and HSC-CM cultured HCC cells

Since both MIR4435-2HG and miR-506-3p can reverse HSC-CM effects on TGF- β /Smad signaling and HCC cell phenotype, the present study evaluated the dynamic effects of the MIR4435-2HG/miR-506-3p on TGF- β 1 and Hep3B cells to investigate whether MIR4435-2HG mediates HSC-CM effects on HCC cells through miR-506-3p and its target TGFB1. Hep3B cells were co-transfected with si-MIR4435-2HG and antagomir-506-3p, and with HSC-CM to detect the cell phenotypes. Under HSC-CM, the silencing of MIR4435-2HG inhibited, whereas the inhibition of miR-506-3p enhanced the migration and invasion of HCC cells. The miR-506-3p inhibition significantly attenuated the effects of MIR4435-2HG silencing (Figure 5A,B). MIR4435-2HG silencing upregulated E-cadherin and downregulate vimentin, TGF- β 1 and ZEB1 expression, and inhibited Smad2 and Smad3 phosphorylation, whereas miR-506-3p inhibition dramatically attenuated the effects of MIR4435-2HG silencing on EMT biomarkers and TGF- β /Smad signaling (Figure 5C,D). These data confirmed the hypothesis that MIR4435-2HG mediates HSC-CM effects on HCC cells through miR-506-3p and its downstream TGFB1.

3.8 | HSCs function on HCC cells through releasing CXCL1

Since the MIR4435-2HG/miR-506-3p/TGFB1 axis mediates HSC-CM effects on HCC cells, next we continued to investigate the way in which HSC-CM induces MIR4435-2HG upregulation in HCC cells. According to a previous study,¹⁹ HSCs are the most influential stromal regulators of HCC. Furthermore, PGF,²⁰ CXCL1,^{21,22} IGF2,^{23,24} CSF1,²⁵ and HGF^{26,27} have been reported to be closely associated with HSC activation, therefore we examined the levels of PGF, CXCL1, IGF2, CSF1, and HGF in cancerous and paracancerous samples. Figure 6A showed that CXCL1 mRNA expression was sharply increased in cancer samples compared with that in paracancerous samples. Then, we transfected HSCs with si-CXCL1, and determined CXCL1 levels in the culture medium via ELISA; as shown in Figure 6B, si-CXCL1 transfection significantly decreased the levels of CXCL1 in the culture medium.

Then, we cultured HCC cells with HSCs transfected with si-NC, and transfected HSCs with si-CXCL1 or control CM containing recombinant CXCL1 protein (rCXCL1-CM), and measured MIR4435-2HG and miR-506-3p expression within HCCs. Compared with HCC cells cultured with si-NC CM, si-CXCL1 CM significantly downregulated MIR4435-2HG and upregulated miR-506-3p, whereas rCXCL1-CM upregulated MIR4435-2HG and downregulated miR-506-3p (Figure 6C,D). As for cellular functions, si-NC CM and si-CXCL1 CM significantly inhibited, whereas rCXCL1-CM promoted cell migration and cell invasion (Figure 6E,F). As for EMT biomarkers and the TGF- β /Smad pathway, si-CXCL1 CM increased E-cadherin and decreased vimentin, TGF- β 1, and ZEB1 protein contents and inhibited Smad2 and Smad3 phosphorylation, whereas rCXCL1-CM exerted opposite effects on these proteins (Figure 6G). HSCs might affect HCC cells by releasing CXCL1.

3.9 | Dynamic effects of MIR4435-2HG and HSC-released CXCL1 on an orthotopic xenotransplanted tumor model of HCC in mice

Concerning the in vivo effects of HSC-released CXCL1, an orthotopic xenotransplanted tumor model of HCC was established in mice

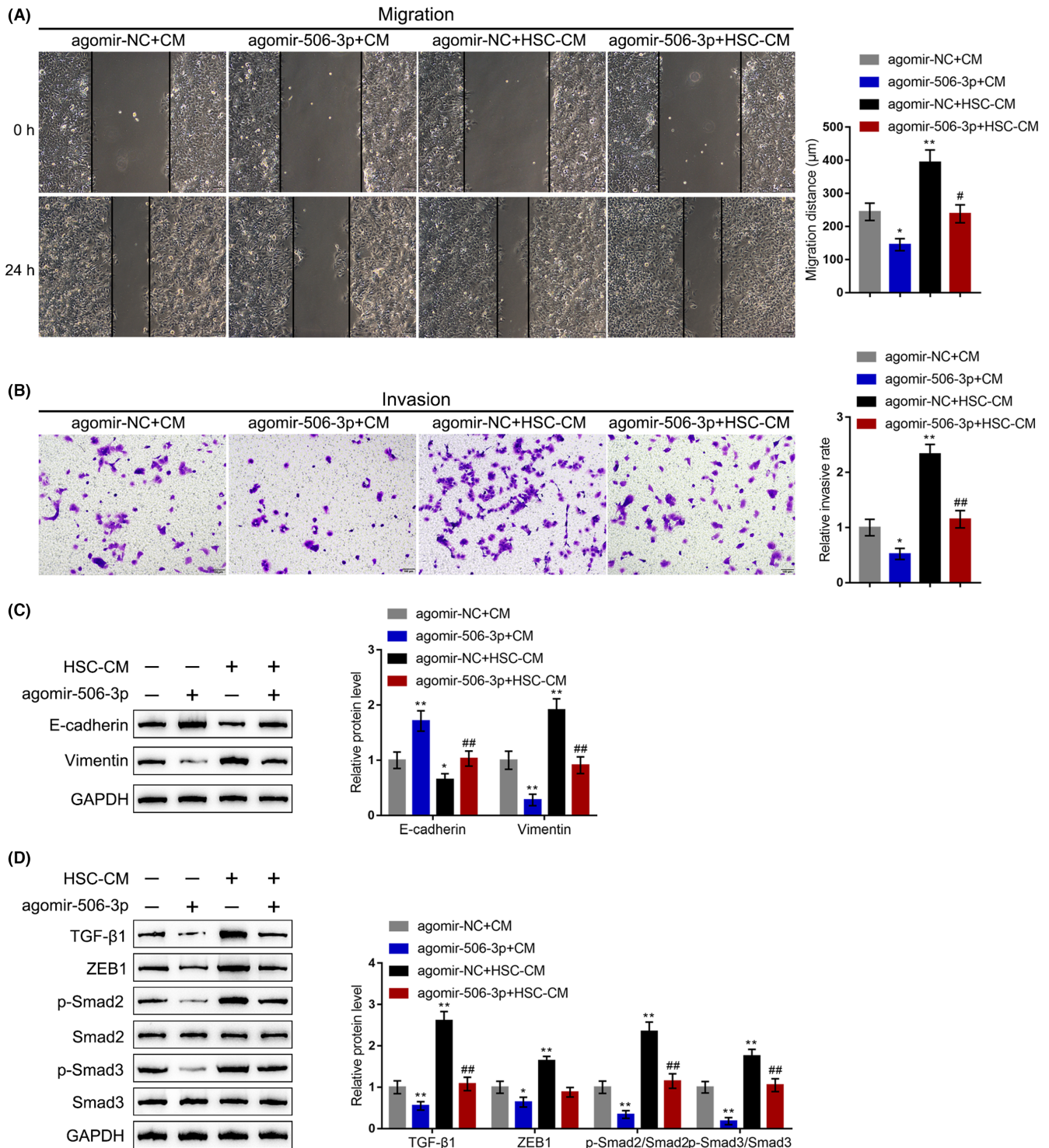


FIGURE 4 miR-506-3p overexpression attenuates the effects of HSC-CM on HCC cells. Hep3B cells were transfected with agomir-NC or agomir-506-3p, cultured with CM or HSC-CM, and examined for cell migration by wound healing assay (A). Cell invasion by Transwell assay (B). Protein levels of E-cadherin and vimentin by immunoblotting (C) and protein levels of TGF- β 1, ZEB1, p-Smad2, Smad2, p-Smad3, and Smad3 by immunoblotting (D). * $p < 0.05$, ** $p < 0.01$, compared with the agomir-NC+CM group; # $p < 0.05$, ## $p < 0.01$, compared with the agomir-NC+HSC-CM group.

by injecting HSCs and transduced Hep3B cells. To further confirm the function of CXCL1, the receptor of CXCL1 (CXCR2) was knocked down in Hep3B cells. Hep3B cells were transfected with si-NC, si-CXCR2 1/2/3 for 48h, and the transduction efficiency was

confirmed using immunoblotting; due to the best interfering efficiency, si-CXCR2 2 was chosen as the sequence used for lentivirus construction and used for the following experiments (Figure 7A). The mice were divided into three groups, Hep3B cells (transduced

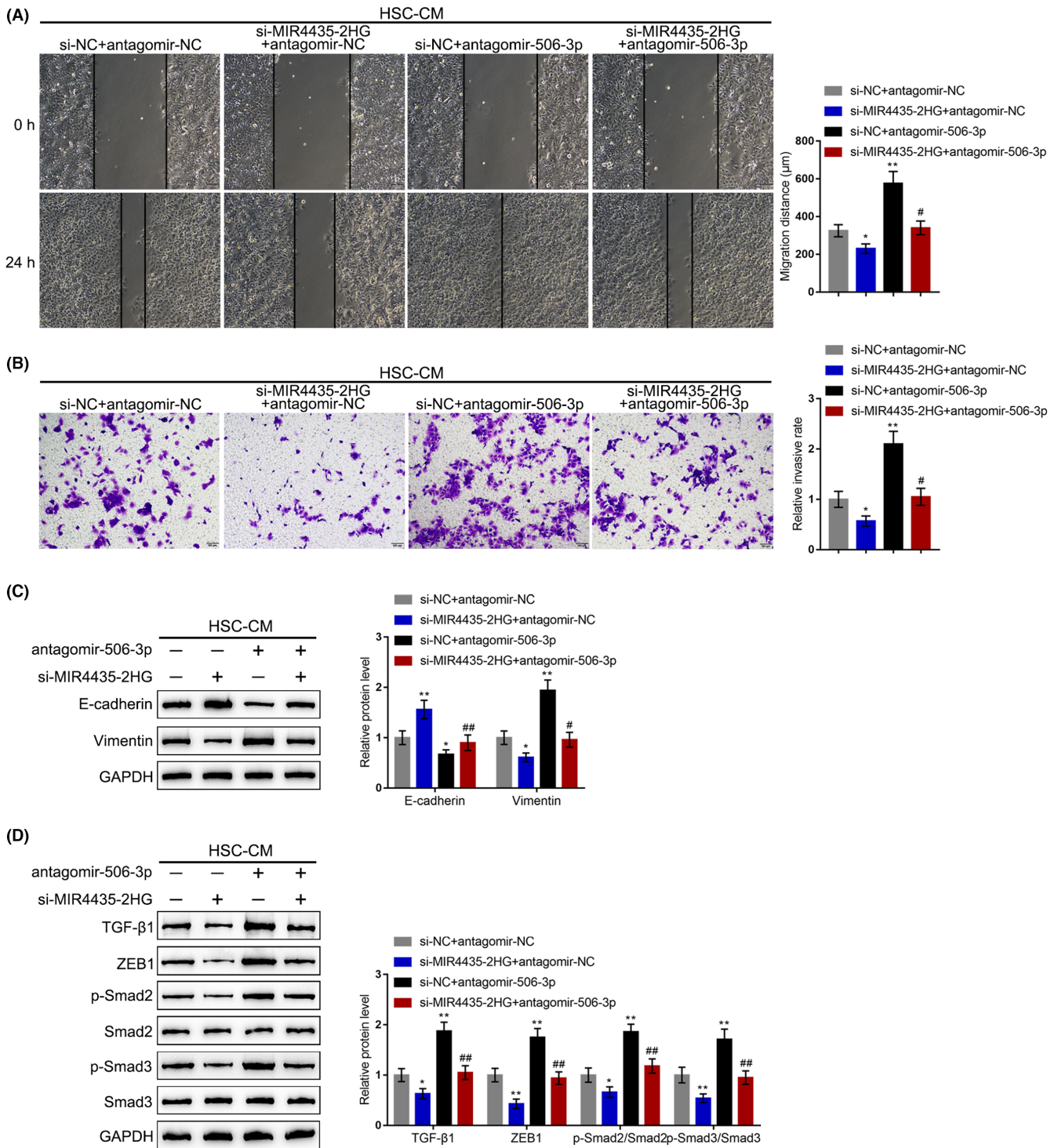


FIGURE 5 Dynamic effects of MIR4435-2H and miR-506-3p on TGF-β1 and HSC-CM cultured HCC cells. Hep3B cells were co-transfected with si-MIR4435-2HG and antagomir-506-3p, cultured with HSC-CM, and examined for cell migration by wound healing assay (A). Cell invasion by Transwell assay (B). Protein levels of E-cadherin and vimentin by immunoblotting (C), and protein levels of TGF-β1, ZEB1, p-Smad2, Smad2, p-Smad3, and Smad3 by immunoblotting (D). * $p < 0.05$, ** $p < 0.01$, compared with the si-NC + antagomir-NC group; # $p < 0.05$, ## $p < 0.01$, compared with the si-NC + antagomir-506-3p group.

with lv-sh-NC)+HSC group ($n = 6$), Hep3B cells (transduced with sh-lv-CXCR2)+HSC group ($n = 6$), and Hep3B cells (transduced with lv-sh-CXCR2 + MIR4435-2HG)+HSC group ($n = 6$), and injected with a mixture of HSCs and transduced Hep3B cells accordingly. **Figure 7B**

shows that the tumor number derived from the mixture of HSCs and Hep3B cells transduced with lv-sh-CXCR2 was lower compared with the control group, whereas Hep3B cells co-transduced with lv-sh-CXCR2 and MIR4435-2HG significantly increased the tumor

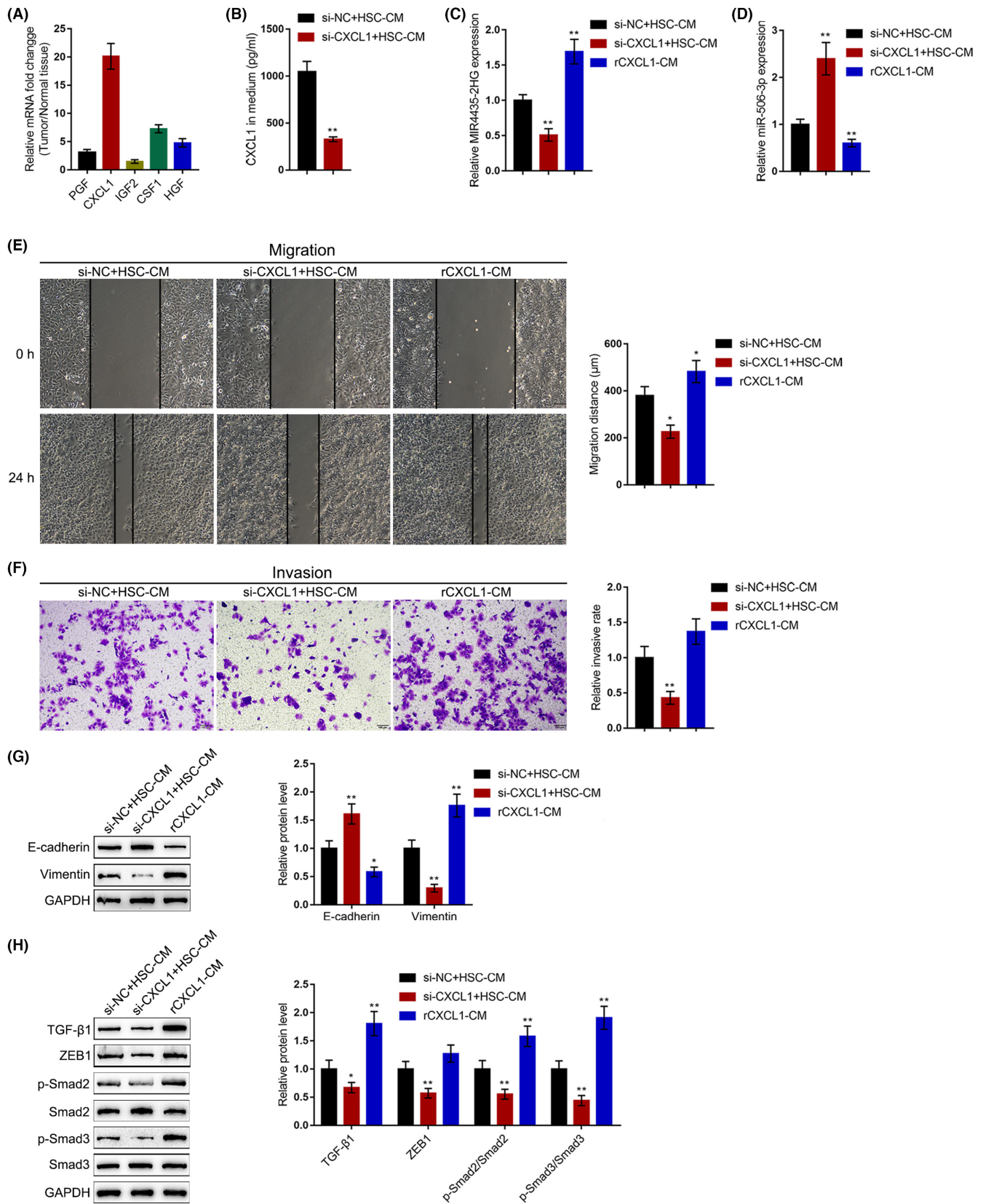


FIGURE 6 HSCs function on HCC cells through releasing CXCL1. (A) The mRNA expression levels of PGF, CXCL1, IGF2, CSF1, and HGF in HSCs were examined by qRT-PCR. (B) HSCs were transfected with si-CXCL1 and examined for the CXCL1 levels in the culture medium by ELISA. HCCs were cultured with HSCs transfected with si-NC, HSCs transfected with si-CXCL1, or control CM added with recombinant CXCL1 (rCXCL1-CM). Then, the expression levels of MIR4435-2HG and miR-506-3p were determined by qRT-PCR (C, D). Cell migration was examined by wound healing assay (E). Cell invasion was examined by Transwell assay (F). The protein levels of E-cadherin and vimentin were examined by immunoblotting (G). The protein levels of TGF- β 1, ZEB1, p-Smad2, Smad2, p-Smad3, and Smad3 were examined by immunoblotting (H). * $p < 0.05$, ** $p < 0.01$, compared with the si-NC + HSC-CM group.

number. Consistently, IF staining confirmed the existence of HCC cells (AFP positive) and activated HSC (α -SMA). The fluorescent signals representing AFP and α -SMA in the Hep3B cells (transduced

with lv-sh-CXCR2)+HSC group were the weakest (Figure 7C) and were partially restored in the Hep3B cells (transduced with lv-sh-CXCR2+MIR4435-2HG)+HSC group. Moreover, in the Hep3B

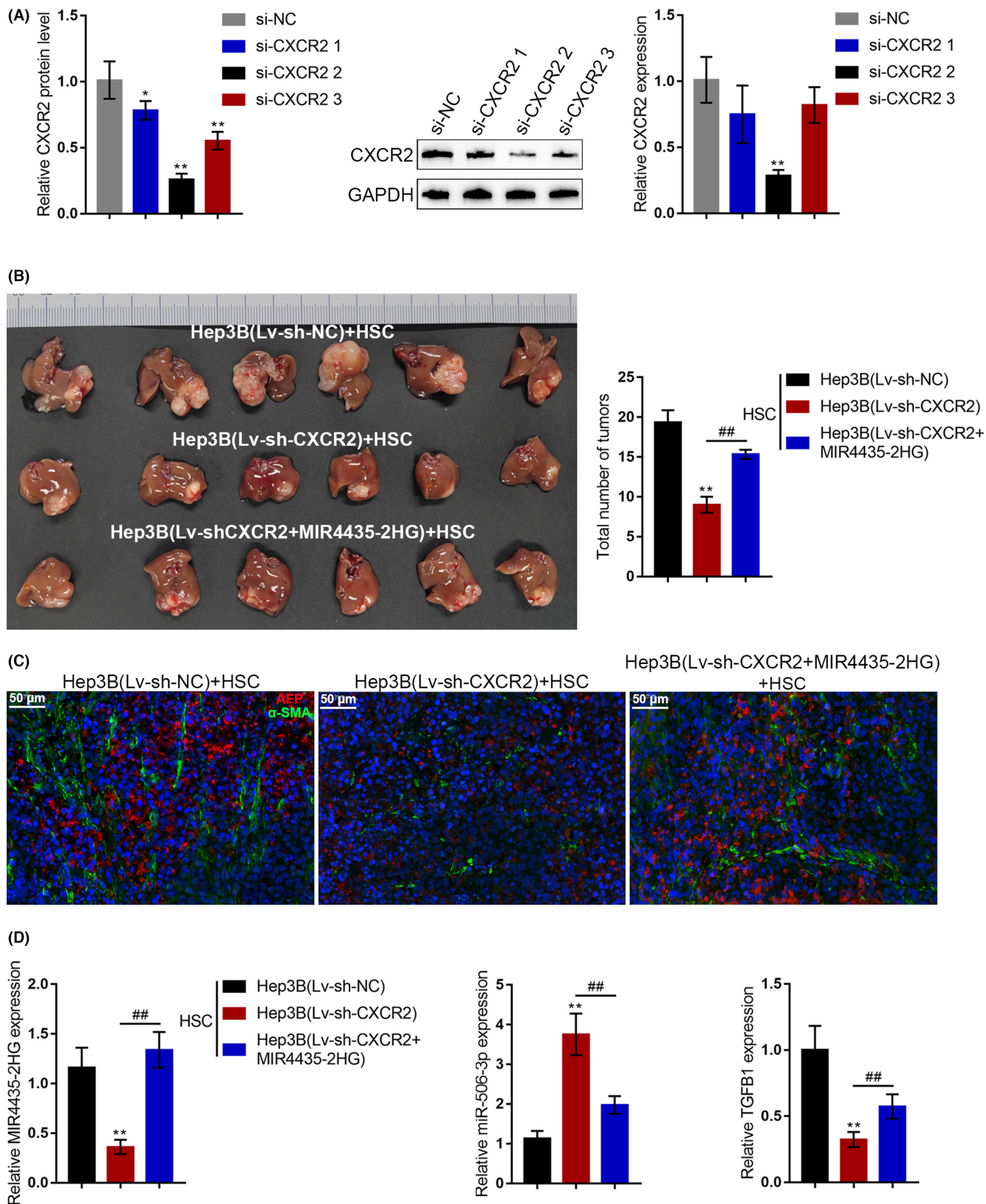


FIGURE 7 Legend on next page

FIGURE 7 Dynamic effects of MIR4435-2HG and HSC-released CXCL1 on an orthotopic xenotransplanted tumor model of HCC in mice. (A) Hep3B cells were transfected with si-NC, si-CXCR2 1/2/3 for 48 h and the transduction efficiency was confirmed using immunoblotting. si-CXCR2 2 was chosen as the sequence used for lentivirus construction and used in following experiments because of the best interfering efficiency. (B–D) An orthotopic xenotransplanted tumor model of HCC was established in mice by injecting HSCs and transduced Hep3B cells. Mice were divided into three groups: the Hep3B cells (transduced with lv-sh-NC) + HSC group ($n = 6$), the Hep3B cells (transduced with lv-sh-CXCR2) + HSC group ($n = 6$), the Hep3B cells (transduced with lv-sh-CXCR2 + MIR4435-2HG) + HSC group ($n = 6$), and injected with a mixture of HSCs and transduced Hep3B cells accordingly. (B) Tumor numbers were monitored in each group. (C) Double-labeling immunofluorescence for AFP (HCC cell marker) and α -SMA (hepatic stellate cell activation marker) labeling was performed. (D) The expression levels of MIR4435-2HG, miR-506-3p, and TGFB1 in tumor samples were examined using qRT-PCR. * $p < 0.05$, ** $p < 0.01$.

cells (transduced with lv-sh-CXCR2) + HSC group, MIR4435-2HG and TGFB1 expression were the lowest, whereas miR-506-3p expression peaked among the three groups (Figure 7D). In the Hep3B cells (transduced with lv-sh-CXCR2 + MIR4435-2HG) + HSC group, MIR4435-2HG and TGFB1 expression was partially elevated, whereas miR-506-3p expression was partially downregulated compared with the Hep3B cells (transduced with lv-sh-CXCR2) + HSC group. These results indicated that the CXCL1/CXCR2 axis was involved in the HSC-induced malignant behavior and aberrant upregulation of MIR4435-2HG in HCC cells.

3.10 | CXCL1, TGF- β 1, MIR4435-2HG, and miR-506-3p levels within tissue samples

Finally, CXCL1, TGF- β 1, MIR4435-2HG, and miR-506-3p levels in tissue samples were examined as a further confirmation of the above in vitro findings. HCC tissues and adjacent normal control tissues were collected for H&E staining to confirm the histopathological features (Figure 8A). The double-labeling immunofluorescence of AFP (HCC cell marker) and α -SMA (hepatic stellate cell activation marker) confirmed that hepatic stellate cells were activated in HCC tissues compared to adjacent normal control tissues (Figure 8B). In HCC tissue samples, the levels of CXCL1 and TGF- β 1 were higher than those in adjacent normal control tissues (Figure 8C,D). Moreover, compared with adjacent normal control tissues, MIR4435-2HG expression was shown to be increased and miR-506-3p expression decreased within HCC tissues (Figure 8E,F). According to TCGA data, MIR4435-2HG expression was significantly higher in HCC tissue samples compared with normal control (Figure 8G). Moreover, also based on TCGA-liver hepatocellular carcinoma (LIHC) data, patients with higher MIR4435-2HG expression had a significantly worse prognosis compared with those with lower MIR4435-2HG expression (Figure 8H).

4 | DISCUSSION

In the present study, we identified TGF- β signaling as a critical signaling pathway in Hep3B cells cultured in HSC-CM and MIR4435-2HG as a hub lncRNA associated with TGF- β signaling and HSC activation. HSC-CM culture could induce HCC cell malignant behaviors, partially reversed by MIR4435-2HG silencing. miR-506-3p directly binds to MIR4435-2HG and the 3'UTR of TGFB1 in HCC cells.

Similarly, miR-506-3p overexpression also attenuated HSC-CM-induced behaviors of HCC cell malignant. In HSC-CM cultured HCC cells, the effects of MIR4435-2HG knockdown on TGFB1 expression and HCC cell phenotypes were partially reversed by miR-506-3p inhibition. HSCs affected HCC cell phenotypes by releasing CXCL1. In an orthotopic xenotransplanted tumor model of HCC in mice, CXCR2 knockdown in HCC cells significantly inhibited tumorigenesis, which was partially reversed by MIR4435-2HG overexpression in HCC cells. In HCC tissue samples, the levels of CXCL1, TGF- β 1, and MIR4435-2HG were upregulated, whereas miR-506-3p expression was downregulated.

Smad proteins are intracellular signaling molecules of the TGF- β superfamily²⁸ that exert a critical effect on the activation of HSCs and subsequent liver fibrosis, liver cirrhosis, and even HCC. After HSC activation, the expression level and the production of TGF- β 1 increase, which acts as an autocrine factor for stimulating fibrogenic extracellular matrix production and perpetuation of HSC activation.²⁹ Consistent with the above findings, differentially expressed gene analysis based on GSE62455 indicated that differentially expressed genes in HCC cells in response to HSC-CM were significantly enriched in TGF- β signaling and downstream EMT signaling. Using WGCNA, lncRNA MIR4435-2HG was recognized as a hub lncRNA in HCC cells in response to HSC-CM. More importantly, MIR4435-2HG exhibited the same expression trend as TGFB1 and was significantly correlated with TGFB1, suggesting that MIR4435-2HG might mediate TGF- β -induced HSC activation and HSC-CM functions on HCC cells.

MIR4435-2HG was abnormally upregulated within several cancers, such as lung cancer,^{30,31} colorectal cancer,^{32,33} gastric cancer,³⁴ and prostate carcinoma.³⁵ Interestingly, studies on lung cancer³¹ and prostate carcinoma³⁵ both indicated the same expression trend of MIR4435-2HG and TGF- β 1 in tumor tissue samples. In HCC, although abnormal upregulation of MIR4435-2HG has also been reported,^{36,37} the reason why MIR4435-2HG was upregulated within HCC has not yet been fully determined. Herein, both bioinformatics and experimental analyses indicated the upregulation of MIR4435-2HG might be a consequence of the HSC-CM culture condition. This speculation was evidenced by in vitro findings that HSC-CM culturing significantly promoted HCC cell aggressiveness, increased the levels of mesenchymal marker vimentin, and induced the activation of the TGF- β /Smad signaling, whereas silencing MIR4435-2HG in HCC cells reversed these changes caused by HSC-CM culturing.

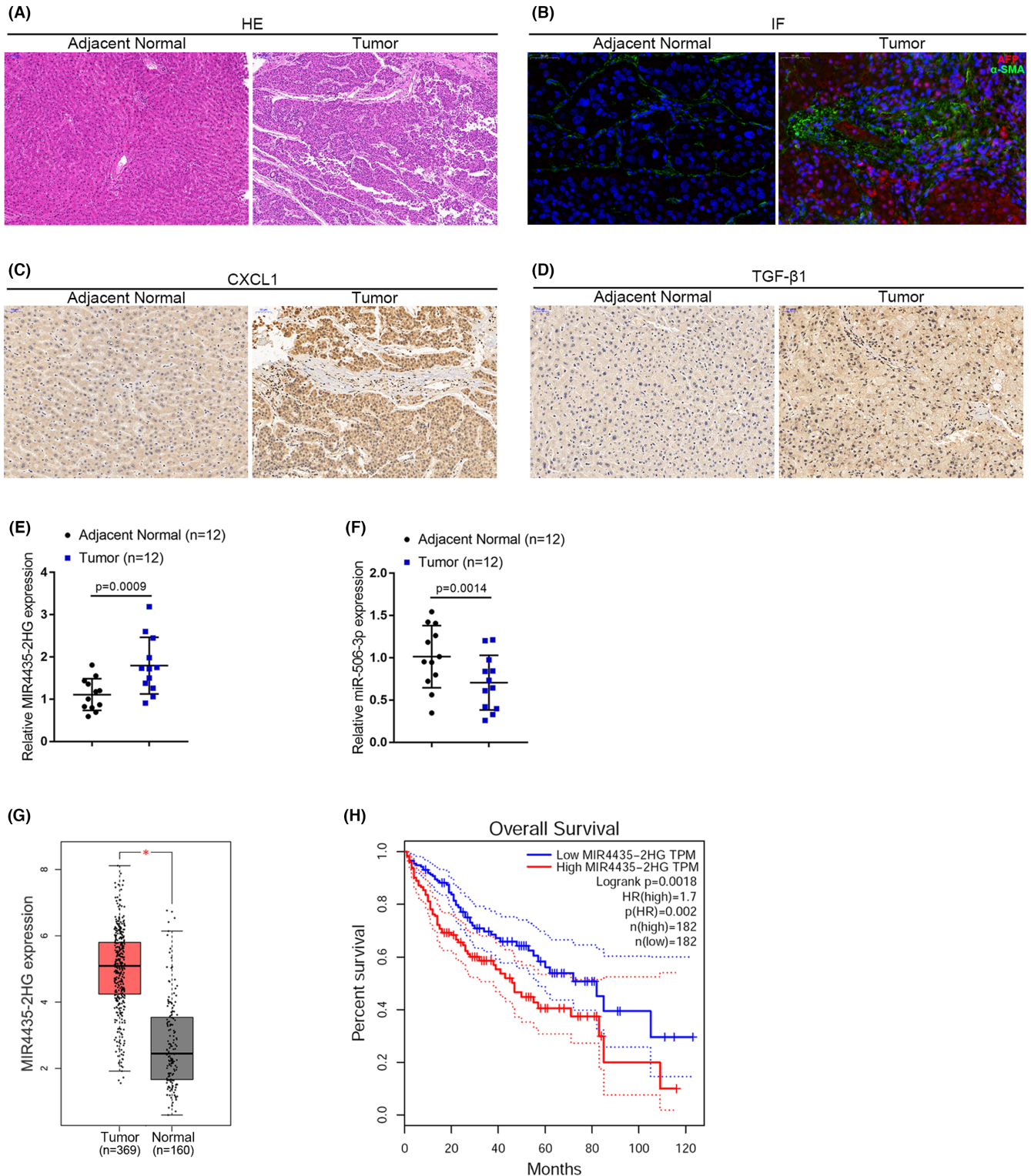


FIGURE 8 Levels of CXCL1, TGF- β 1, MIR4435-2HG, and miR-506-3p in tissue samples. (A) HCC and adjacent noncancerous tissue samples were collected and the histopathological characteristics were confirmed by H&E staining. (B) Double-labeling immunofluorescence for AFP (HCC cell marker) and α -SMA (hepatic stellate cell activation marker) labeling was performed. (C, D) The levels of CXCL1 and TGF- β 1 in tissue samples were examined by immunohistochemical (IHC) staining. (E, F) The expression levels of MIR4435-2HG and miR-506-3p in tissue samples were examined by qRT-PCR. (G) The expression levels of MIR4435-2HG in tumor and normal samples according to TCGA-LIHC data. (H) The correlation of MIR4435-2HG with HCC patients' prognosis was analyzed based on TCGA data.

miRNAs have attracted increasing attention because of their role in mediating the crosstalk between lncRNAs and mRNAs.^{15,16} Kong et al.³⁷ found that MIR4435-2HG upregulated miR-487a to

promote the capacity of tumor cells to proliferate. Herein, considering the significant association between MIR4435-2HG and TGF β 1 expression, we searched for miRNAs that might mediate

the crosstalk between MIR4435-2HG and TGFB1, and found miR-506-3p. Previously, it was reported that miR-506-3p exerted tumor-suppressive effects on cancers, including HCC.³⁸ miR-506-3p served as a tumor suppressor by targeting TGFB1 in colorectal cancer.³⁹ Under HSC-CM culturing, miR-506-3p overexpression in HCC cells significantly reversed HSC-CM-induced HCC cell aggressiveness, increased vimentin, and activated the TGF- β /Smad pathway, confirming its tumor-suppressive effect in HCC. More importantly, under HSC-CM culturing, miR-506-3p inhibition within HCC cells reversed the effects of MIR4435-2HG silencing, indicating that miR-506-3p was downstream of MIR4435-2HG and MIR4435-2HG mediated the role of HSC-MC affecting HCC cells through the miR-506-3p/TGFB1 axis.

Since HSC released soluble cytokines, chemokines, and chemotaxis, forming a complex tumor microenvironment,³ we speculated that HSC-released agents might be responsible for the aberrant upregulation of MIR4435-2HG in HCC cells. CXCL1 was considered as a key factor with critical functions in HCC initiation^{40,41} and development.⁴² Herein, after silencing CXCL1 in HSCs, the conditioned CM could no longer induce MIR4435-2HG upregulation and miR-506-3p downregulation, the aggressiveness of HCC cells, and the TGF- β /Smad pathway activation within HCCs. However, after adding rCXCL1 to the culture medium, the effects of HSC-CM on MIR4435-2HG expression and miR-506-3p expression, as well as oncogenic effects on HCC cells, were even enhanced. More importantly, an orthotopic xenotransplanted tumor model of HCC was established in mice by injecting a mixture of HSCs and differentially transduced HCC cells. CXCR2 knockdown in HCC cells significantly inhibited tumorigenesis, whereas MIR4435-2HG overexpression in HCC cells partially restored the tumorigenesis, suggesting that blocking the CXCL1/CXCR2 could inhibit the tumorigenesis in the mice model, whereas overexpressing MIR4435-2HG in HCC cells partially attenuated the inhibitory effects. These data suggest that HSC-secreted CXCL1 might be the reason for the aberrant upregulation of MIR4435-2HG in HCC cells. However, the specific mechanism of upregulation of MIR4435-2HG by secreted CXCL1 needs to be further investigated.

In conclusion, HSC-released CXCL1 aggravates HCC cell malignant behaviors through the MIR4435-2HG/miR-506-3p/TGFB1 axis (Figure S4). In addition to CXCL1, the MIR4435-2HG/miR-506-3p/TGFB1 axis might also be an underlying target for HCC therapy.

AUTHOR CONTRIBUTIONS

Shaling Li: Conceptualization, writing – original draft, funding acquisition. Xingwang Hu: Data curation. Songman Yu: Formal analysis. Panpan Yi: Methodology. Ruochan Chen: Software. Zebing Huang: Resources. Yan Huang: Visualization. Yun Huang: Investigation. Rongrong Zhou: Writing – review & editing, project administration. Xue-gong Fan: Funding acquisition, supervision.

ACKNOWLEDGMENT

None.

FUNDING INFORMATION

This study was supported by the National Nature Science Foundation of China (81970523), the National Nature Science Foundation of Hunan, China (2020JJ4877 and 2020JJ4932), and the Ministry of Science and Technology International Cooperation Project (2015DFA31490).

DISCLOSURE

The authors declare that they have no conflict of interest.

ETHICS STATEMENT

All procedures performed in studies involving human participants were in accordance with the ethical standards of Xiangya Hospital and with the 1964 Helsinki declaration. Informed consent to participate in the study was obtained from participants. All animal experiments comply with the Guidelines for the Care and Use of Experimental Animals and are approved by the Experimental Animal Committee of the Xiangya Hospital.

ORCID

Shaling Li  <https://orcid.org/0000-0002-4568-7198>

REFERENCES

1. El-Serag HB. Hepatocellular carcinoma. *N Engl J Med.* 2011;365:1118-1127.
2. Yang JD, Nakamura I, Roberts LR. The tumor microenvironment in hepatocellular carcinoma: current status and therapeutic targets. *Semin Cancer Biol.* 2011;21:35-43.
3. Friedman SL. Hepatic stellate cells: protean, multifunctional, and enigmatic cells of the liver. *Physiol Rev.* 2008;88:125-172.
4. Amann T, Bataille F, Spruss T, et al. Activated hepatic stellate cells promote tumorigenicity of hepatocellular carcinoma. *Cancer Sci.* 2009;100:646-653.
5. Wang BB, Cheng JY, Gao HH, Zhang Y, Chen ZN, Bian H. Hepatic stellate cells in inflammation-fibrosis-carcinoma axis. *Anat Rec (Hoboken).* 2010;293:1492-1496.
6. Gressner AM, Weiskirchen R, Breitkopf K, Dooley S. Roles of TGF- β in hepatic fibrosis. *Front Biosci.* 2002;7:d793-d807.
7. Swartz MA, Iida N, Roberts EW, et al. Tumor microenvironment complexity: emerging roles in cancer therapy. *Cancer Res.* 2012;72:2473-2480.
8. Gao D, Vahdat LT, Wong S, Chang JC, Mittal V. Microenvironmental regulation of epithelial-mesenchymal transitions in cancer. *Cancer Res.* 2012;72:4883-4889.
9. He Y, Meng XM, Huang C, et al. Long noncoding RNAs: novel insights into hepatocellular carcinoma. *Cancer Lett.* 2014;344:20-27.
10. Han TS, Hur K, Cho HS, Ban HS. Epigenetic associations between lncRNA/circRNA and miRNA in hepatocellular carcinoma. *Cancers (Basel).* 2020;12:2622.
11. Esposti DD, Hernandez-Vargas H, Voegelé C, et al. Identification of novel long non-coding RNAs deregulated in hepatocellular carcinoma using RNA-sequencing. *Oncotarget.* 2016;7:31862-31877.
12. Yin L, Cai Z, Zhu B, Xu C. Identification of key pathways and genes in the dynamic progression of HCC based on WGCNA. *Genes (Basel).* 2018;9:92.
13. Dewidar B, Meyer C, Dooley S, Meindl-Beinker AN. TGF- β in hepatic stellate cell activation and liver fibrogenesis-updated 2019. *Cell.* 2019;8:1419.

14. Tsuchida T, Friedman SL. Mechanisms of hepatic stellate cell activation. *Nat Rev Gastroenterol Hepatol*. 2017;14:397-411.
15. Tan JY, Marques AC. The miRNA-mediated cross-talk between transcripts provides a novel layer of posttranscriptional regulation. *Adv Genet*. 2014;85:149-199.
16. Ergun S, Oztuzcu S. Oncocers: ceRNA-mediated cross-talk by sponging miRNAs in oncogenic pathways. *Tumour Biol*. 2015;36:3129-3136.
17. Chu K, Gu J. microRNA-103a-3p promotes inflammation and fibrosis in nonalcoholic fatty liver disease by targeting HBP1. *Immunopharmacol Immunotoxicol*. 2022;28:1-11.
18. Guo Z, Zhang W, Xia G, et al. Sp1 upregulates the four and half lim 2 (FHL2) expression in gastrointestinal cancers through transcription regulation. *Mol Carcinog*. 2010;49:826-836.
19. Engelmann JC, Amann T, Ott-Rotzer B, et al. Causal modeling of cancer-stromal communication identifies PAPP A as a novel stroma-secreted factor activating NFkappaB signaling in hepatocellular carcinoma. *PLoS Comput Biol*. 2015;11:e1004293.
20. Liu Z, Chen M, Zhao R, et al. CAF-induced placental growth factor facilitates neoangiogenesis in hepatocellular carcinoma. *Acta Biochim Biophys Sin Shanghai*. 2020;52:18-25.
21. Shi WP, Ju D, Li H, et al. CD147 promotes CXCL1 expression and modulates liver fibrogenesis. *Int J Mol Sci*. 2018;19:1145.
22. Zhou Z, Xu MJ, Cai Y, et al. Neutrophil-hepatic stellate cell interactions promote fibrosis in experimental steatohepatitis. *Cell Mol Gastroenterol Hepatol*. 2018;5:399-413.
23. Mousavi SA, Fonhus MS, Kindberg GM, Tolleshaug H, Berg T. Enhanced activity of lysosomal proteases in activated rat hepatic stellate cells is associated with a concomitant increase in the number of the mannose-6-phosphate/insulin-like growth factor II receptor. *Cell Biol Int*. 2013;37:703-712.
24. Weber F, Casalini T, Valentino G, et al. Targeting transdifferentiated hepatic stellate cells and monitoring the hepatic fibrogenic process by means of IGF2R-specific peptides designed in silico. *J Mater Chem B*. 2021;9:2092-2106.
25. Konishi T, Schuster RM, Goetzman HS, Caldwell CC, Lentsch AB. Fibrotic liver has prompt recovery after ischemia-reperfusion injury. *Am J Physiol Gastrointest Liver Physiol*. 2020;318:G390-G400.
26. Ma PF, Gao CC, Yi J, et al. Cytotherapy with M1-polarized macrophages ameliorates liver fibrosis by modulating immune microenvironment in mice. *J Hepatol*. 2017;67:770-779.
27. Narmada BC, Chia SM, Tucker-Kellogg L, Yu H. HGF regulates the activation of TGF-beta1 in rat hepatocytes and hepatic stellate cells. *J Cell Physiol*. 2013;228:393-401.
28. Wrana JL, Attisano L. The Smad pathway. *Cytokine Growth Factor Rev*. 2000;11:5-13.
29. Gong W, Pecci A, Roth S, Lahme B, Beato M, Gressner AM. Transformation-dependent susceptibility of rat hepatic stellate cells to apoptosis induced by soluble Fas ligand. *Hepatology*. 1998;28:492-502.
30. Qian H, Chen L, Huang J, et al. The lncRNA MIR4435-2HG promotes lung cancer progression by activating beta-catenin signaling. *J Mol Med (Berl)*. 2018;96:753-764.
31. Yang M, He X, Huang X, Wang J, He Y, Wei L. LncRNA MIR4435-2HG-mediated upregulation of TGF-beta1 promotes migration and proliferation of nonsmall cell lung cancer cells. *Environ Toxicol*. 2020;35:582-590.
32. Dong X, Yang Z, Yang H, Li D, Qiu X. Long non-coding RNA MIR4435-2HG promotes colorectal cancer proliferation and metastasis through miR-206/YAP1 Axis. *Front Oncol*. 2020;10:160.
33. Ouyang W, Ren L, Liu G, Chi X, Wei H. LncRNA MIR4435-2HG predicts poor prognosis in patients with colorectal cancer. *PeerJ*. 2019;7:e6683.
34. Wang H, Wu M, Lu Y, et al. LncRNA MIR4435-2HG targets desmoplakin and promotes growth and metastasis of gastric cancer by activating Wnt/beta-catenin signaling. *Aging (Albany NY)*. 2019;11:6657-6673.
35. Zhang H, Meng H, Huang X, et al. LncRNA MIR4435-2HG promotes cancer cell migration and invasion in prostate carcinoma by upregulating TGF-beta1. *Oncol Lett*. 2019;18:4016-4021.
36. Wang B, Tang D, Zhang Z, Wang Z. Identification of aberrantly expressed lncRNA and the associated TF-mRNA network in hepatocellular carcinoma. *J Cell Biochem*. 2020;121:1491-1503.
37. Kong Q, Liang C, Jin Y, et al. The lncRNA MIR4435-2HG is upregulated in hepatocellular carcinoma and promotes cancer cell proliferation by upregulating miRNA-487a. *Cell Mol Biol Lett*. 2019;24:26.
38. Liu Y, Yan W, Zhou D, Jin G, Cheng X. Long noncoding RNA HOXA11AS accelerates cell proliferation and epithelial-mesenchymal transition in hepatocellular carcinoma by modulating the miR5063p/slug axis. *Int J Mol Med*. 2020;46:1805-1815.
39. Shang A, Gu C, Wang W, et al. Exosomal circPACRGL promotes progression of colorectal cancer via the miR-142-3p/miR-506-3p-TGF-beta1 axis. *Mol Cancer*. 2020;19:117.
40. Tang KH, Ma S, Lee TK, et al. CD133(+) liver tumor-initiating cells promote tumor angiogenesis, growth, and self-renewal through neurotensin/interleukin-8/CXCL1 signaling. *Hepatology*. 2012;55:807-820.
41. Jiang J, Ye F, Yang X, et al. Peri-tumor associated fibroblasts promote intrahepatic metastasis of hepatocellular carcinoma by recruiting cancer stem cells. *Cancer Lett*. 2017;404:19-28.
42. Cui X, Li Z, Gao J, Gao PJ, Ni YB, Zhu JY. Elevated CXCL1 increases hepatocellular carcinoma aggressiveness and is inhibited by miRNA-200a. *Oncotarget*. 2016;7:65052-65066.

SUPPORTING INFORMATION

Additional supporting information can be found online in the Supporting Information section at the end of this article.

How to cite this article: Li S, Hu X, Yu S, et al. Hepatic stellate cell-released CXCL1 aggravates HCC malignant behaviors through the MIR4435-2HG/miR-506-3p/TGFB1 axis. *Cancer Sci*. 2023;114:504-520. doi:[10.1111/cas.15605](https://doi.org/10.1111/cas.15605)